Cerebral Cortex, November 2016;26: 3690–3704

doi: 10.1093/cercor/bhw213
Advance Access Publication Date: 11 July 2016
Original Article

ORIGINAL ARTICLE

Sensory Response of Transplanted Astrocytes in Adult Mammalian Cortex In Vivo

Kuan Zhang[1,†], Chunhai Chen[2,†], Zhiqi Yang[1,3], Wenjing He[1], Xiang Liao[1], Qinlong Ma[2], Ping Deng[2], Jian Lu[1], Jingcheng Li[1], Meng Wang[1], Mingli Li[4], Lianghong Zheng[4], Zhuan Zhou[4], Wei Sun[1], Liting Wang[1], Hongbo Jia[5], Zhengping Yu[2], Zhou Zhou[2], and Xiaowei Chen[1,6]

[1]Brain Research Center, Third Military Medical University, Chongqing 400038, China, [2]Department of Occupational Health, Third Military Medical University, Chongqing 400038, China, [3]Department of Neurology, Lanzhou General Hospital, Lanzhou Military Area Command, Lanzhou, Gansu 730050, China, [4]State Key Laboratory of Biomembrane and Membrane Biotechnology, Institute of Molecular Medicine, Peking-Tsinghua Center for Life Sciences, PKU-IDG/McGovern Institute for Brain Research, Peking University, Beijing 100871, China, [5]Brain Research Instrument Innovation Center, Suzhou Institute of Biomedical Engineering and Technology, Chinese Academy of Sciences, Suzhou 215163, China, and [6]CAS Center for Excellence in Brain Science and Intelligence Technology, Shanghai Institutes for Biological Sciences, Chinese Academy of Sciences, Shanghai 200031, China

Address correspondence to Xiaowei Chen, Brain Research Center, Third Military Medical University, Chongqing 400038, China. Email: xiaowei_chen@tmmu.edu.cn or to Zhou Zhou, Department of Occupational Health, Third Military Medical University, Chongqing 400038, China. Email: lunazhou00@163.com

[†]K.Z. and C.C. contributed equally to this work.

Abstract

Glial precursor transplantation provides a potential therapy for brain disorders. Before its clinical application, experimental evidence needs to indicate that engrafted glial cells are functionally incorporated into the existing circuits and become essential partners of neurons for executing fundamental brain functions. While previous experiments supporting for their functional integration have been obtained under in vitro conditions using slice preparations, in vivo evidence for such integration is still lacking. Here, we utilized in vivo two-photon Ca^{2+} imaging along with immunohistochemistry, fluorescent indicator labeling-based axon tracing and correlated light/electron microscopy to analyze the profiles and the functional status of glial precursor cell-derived astrocytes in adult mouse neocortex. We show that after being transplanted into somatosensory cortex, precursor-derived astrocytes are able to survive for more than a year and respond with Ca^{2+} signals to sensory stimulation. These sensory-evoked responses are mediated by functionally-expressed nicotinic receptors and newly-established synaptic contacts with the host cholinergic afferents. Our results provide in vivo evidence for a functional integration of transplanted astrocytes into adult mammalian neocortex, representing a proof-of-principle for sensory cortex remodeling through addition of essential neural elements. Moreover, we provide strong support for the use of glial precursor transplantation to understand glia-related neural development in vivo.

Key words: glial precursor transplantation, two-photon Ca^{2+} imaging, astrocytes, somatosensory cortex, sensory response

Introduction

Astrocytes, the major population of glial cells in the brain, are increasingly considered to be the core elements in neural circuits responsible for the control of brain functions through extensive contacts with both neurons and cerebral blood vessels (Eroglu and Barres 2010; Halassa and Haydon 2010). For example, during sensory information processing, astrocytes in the brain respond to surrounding neural activity by increasing intracellular Ca^{2+} signals (Wang et al. 2006; Bekar et al. 2008; Schummers et al. 2008; Ghosh et al. 2013) and likely regulate neuronal activity by releasing Ca^{2+}-dependent gliotransmitter (Parpura et al. 1994; Chen et al. 2005; Eroglu and Barres 2010; Halassa and Haydon 2010; Panatier et al. 2011; Navarrete et al. 2013). Such direct bidirectional astrocyte–neuron interactions indicate that the astrocyte responsiveness is topographically aligned to neuronal sensory maps and the brain astrocytes are active participants for information processing and integration (see review Lopez-Hidalgo and Schummers 2014).

An impairment of astrocyte functions occurs in aging as well as in many neurological and psychiatric disorders in both animal models and patients (Seifert et al. 2006; Kuchibhotla et al. 2009). This strongly suggests that cell transplantation and subsequent integration into the diseased brain circuits would be a potential therapy for these astrocyte-related disorders (Lindvall and Kokaia 2006; Goldman et al. 2012). Indeed, accumulating evidence indicates that transplantation-based cell therapy using glial progenitors or cultured astrocytes efficiently improves brain functions and behaviors in both healthy and diseased conditions (Muller and Best 1989; Lepore et al. 2008; Han et al. 2013; Jiang et al. 2013; Chen et al. 2015). These behavioral outcomes caused by glia transplantation require the functional incorporation of engrafted cells into the recipient networks. Previous in vitro studies have suggested that engrafted astrocytes express the similar molecular and morphological features to their host counterparts (Muller and Best 1989; Lepore et al. 2008; Davies et al. 2011; Han et al. 2013; Jiang et al. 2013; Chen et al. 2015). However, the functional demonstrations for their integration were mainly restricted to the in vitro experiments using brain slice preparations and showed that engrafted astrocytes were able to modulate synaptic transmission (Han et al. 2013; Jiang et al. 2013). Therefore, how transplanted astrocytes are incorporated into the host neural circuits and whether these astrocytes can eventually execute basic brain functions like sensory information processing require further in vivo investigation.

Since Ca^{2+} signaling is considered as a primary form of cellular responsiveness in astrocytes, the application of two-photon Ca^{2+} imaging in conjunction with the use of improved fluorescent Ca^{2+} indicators provides an ideal way for the analysis of astrocyte activity (Hirase et al. 2004; Nimmerjahn et al. 2004; Wang et al. 2009; Volterra et al. 2014). Here, we applied this approach to monitor the functional status of engrafted astrocytes and their responses to sensory stimulation at different time points after transplantation in the living mice. We found that transplanted glial precursor cells derived from embryonic neural stem cells (NSCs) into the adult somatosensory cortex could develop into astrocytes that were able to survive for more than a year, nearly as long as the life span of mice, and express molecular and morphological features of mature cortical astrocytes. We also found that engrafted astrocytes in the adult sensory cortex responded with Ca^{2+} signals to sensory stimulation, suggesting a functional integration into the sensory circuits for executing sensory information processing. Furthermore, we found that the sensory-evoked Ca^{2+} responses in engrafted astrocytes were dependent on the functional expression of nicotinic acetylcholine receptors (nAchRs) and the formation of synapse-like contacts with host cholinergic afferents from the basal forebrain. Thus, these results unveil glial precursor transplantation in the adult brain as an effective strategy for sensory cortex remodeling through a functional incorporation into the existing astrocyte–neuron circuits.

Materials and Methods

Animals

All animal experimental procedures were performed in accordance with institutional animal welfare guidelines and were approved by the Third Military Medical University Animal Care and Use Committee. Embryonic donor tissue was produced by crossing male and female homozygous enhanced green fluorescent protein-expressing (EGFP) mice (FVB.Cg-Tg(CAG-EGFP) B5Nagy/J; stock number: 003516; Jackson Laboratory). The mice receiving transplantation were aged 2–4 months and also FVB/N line.

Embryonic NSC Culture and Astrocyte Precursor Cell Induction

Timed pregnant EGFP mice were used to prepare cortical NSC cultures as previously described with some modifications (Mi et al. 2005; Lakoma et al. 2011). Briefly, E14–E15 mouse cortices were dissected and mechanically dissociated. The dissociated cells were cultured in the serum-free neurosphere culture medium containing 1:1 (v/v) a mixture of Dulbecco's modified Eagle's medium (DMEM) and F12 medium supplemented with B27 (Gibco), FGF2 (20 ng/mL, Sigma), and epidermal growth factor (EGF) (20 ng/mL, Sigma) under floating conditions with half medium changed every 3 days.

For astrocyte precursor cell induction, the formed neurospheres were collected and dissociated using Accutase (eBioscience). The cells were then plated onto poly-L-lysine-coated dishes for attachment. EGF and basic fibroblast growth factor were withdrawn from the culture medium. Ciliary neurotrophic factor (CNTF) (10 ng/mL, Sigma) and 30% fetal bovine serum (FBS) (Gibco) were added to the culture medium to induce NSCs to differentiate into astrocyte precursor cells (Mi and Barres 1999; Barberi et al. 2003; Krencik et al. 2011). After 2 days of induction, the cells were dissociated into single cells and were subsequently used for transplantation.

Cell Transplantation

Concentrated cell suspensions (1×10^5 cells/μL) were loaded into 1 μL Hamilton microsyringe (Neuros Syringe, 65460-02, Hamilton). Microsyringes were positioned at an angle of 45° vertically in a stereotactic injection apparatus (68025, RWD Life Science). The mice were anesthetized throughout the surgery by pentobarbital sodium (1 g/kg). The injections were made into the primary somatosensory cortex (S1) (coordinates: Bregma –0.56 mm, 1.65 mm lateral to midline) at three different depths from the cortical surface: 0.1, 0.3, and 0.5 mm. Approximately 6×10^4 cells in total (200 nL for each depth) were injected at the speed of 10 nL/s using UMP3 microsyringe injector and Micro4 Controller (WPI Inc.). After injections, the needle was remained for an additional 5 min before it was slowly withdrawn from

the cortex. Before and during the injections, the cerebral vessels in the open cranial windows were recorded using a CCD camera (TOUPCAM, TP603100A). After transplantation, the craniotomy sites were marked, and then the incisions were closed with Vetbond tissue adhesive (3 M). Afterwards, the transplanted mice were maintained on a heating pad before they were returned to their cages.

Immunohistochemistry

Engrafted mice were transcardially perfused with 4% paraformaldehyde at different time points after transplantation. The brains were removed, fixed overnight in 4% paraformaldehyde, and cryoprotected in 30% sucrose. Coronal brain sections (40 μm) were cut and stained as described (Panatier et al. 2011). Briefly, floating sections were immunostained with the following primary antibodies: chicken anti-GFP (1:500; Abcam), rabbit anti-GFP (1:500; Abcam), rabbit anti-GFAP (1:300; ZSGB-BIO), goat anti-GFAP (1:500; Abcam), mouse anti-α7-nAchR (1: 300; Sigma), rabbit anti-mGluR1 (1:500; Abcam), rabbit anti-mGluR5 (1:500; Abcam), mouse anti-ChAT (1:500; Abcam), rabbit anti-Syn (1:500; Millipore), rabbit anti-CX30 (1:500; Invitrogen), rabbit anti-A2B5 (1:1000, Abcam), rabbit anti-Nestin (1:300, ZSGB-BIO), mouse anti-NeuN (1:300, ZSGB-BIO), and rabbit anti-D-serine (1:1000, Abcam). The following secondary antibodies were used: Alexa Fluor 488 donkey anti-chicken, Alexa Fluor 568 donkey anti-rabbit, Alexa Fluor 568 donkey anti-mouse, Alexa Fluor 647 donkey anti-goat, and Alexa Fluor 647 donkey anti-mouse (1:500; Molecular Probes). Nuclei were stained with DAPI (4′,6-diamidino-2-phenylindole, 1:10 000, D9564, Sigma-Aldrich). For all immunohistochemical procedures, sections were permeabilized for 30 min in a 1% Triton X-100/PBS solution, and blocked using a solution of 10% normal donkey serum and 0.3% Triton X-100 in PBS for 2 h at room temperature. Sections were incubated in primary antibody solutions overnight at 4 °C, and in secondary antibody solutions for 2 h at room temperature. All primary and secondary antibody incubations were done in 1% normal donkey serum and 0.3% Triton X-100 in PBS. After the primary and secondary antibody incubations were finished, sections were rinsed three times in PBS, and incubated with DAPI for 10 min at room temperature. Then, sections were mounted on glass slides and coverslipped after the second series of washes.

Anterograde Tracing with Mini-Ruby

Projections from nucleus basalis of Meynert were traced with mini-Ruby as described previously (Lai et al. 2012). Briefly, the engrafted mice were anesthetized with atropine and pentobarbital sodium (intraperitoneal; 0.5 mg/mL and 1 mg/mL, respectively, in saline; 100 μL per gram of body weight). Mini-Ruby (Invitrogen), dissolved at a concentration of 5% in water, was injected into nucleus basalis of Meynert (coordinates: Bregma –0.5 mm, 1.5 mm lateral to midline, depth 3.5 mm) through a sharp electrode. Ten to twelve days after the injection, mice were perfused with 4% paraformaldehyde and their brains were postfixed overnight. Brains were sectioned with a freezing microtome at 40 μm.

Confocal Imaging

Histological images were acquired at two zoom factors, ×2 and ×8 at a resolution of 1024 pixels by 1024 pixels with a dwell time of 8 μs per pixel using confocal microscope (Leica SP5) equipped with a ×63 oil immersion objective (NA 1.4). Detailed observation methods are in accordance with the previous study (Panatier et al. 2011). Images were adjusted for brightness and contrast with Adobe Photoshop CS3 (Adobe Systems Inc.).

In Vivo Two-Photon Ca^{2+} Imaging of Cortical Engrafted and Host Astrocytes

For two-photon Ca^{2+} imaging experiments, surgery and recordings were performed as described previously (Stosiek et al. 2003; Chen et al. 2011, 2013). In brief, the mouse was placed onto a warming plate (37–38 °C) and anesthetized by inhalation of 1–1.5% isoflurane (RWD Life Science) in pure O_2. The skin and soft tissues were removed under a dissecting microscope after local application of xylocaine. A custom-made recording chamber was then glued to the skull. A small craniotomy (~1 mm × 1 mm) centered on the previously marked site (coordinates: Bregma –0.56 mm, 1.65 mm lateral to midline) was made. The craniotomy was filled with 1–1.5% low-melting-point agarose to minimize brain pulsations. After surgery, the mouse was transferred into the recording apparatus and the anesthesia level was decreased to 0.5–0.8% isoflurane (breathing rate was around 120 breaths per minute). The recording chamber was perfused with warm artificial cerebrospinal fluid (ACSF) containing (in mM): 125 NaCl, 4.5 KCl, 26 $NaHCO_3$, 1.25 NaH_2PO_4, 2 $CaCl_2$, 1 $MgCl_2$, and 20 glucose, pH 7.4, when bubbled with 95% O_2 and 5% CO_2. The temperature of the mouse was maintained in the range of 36.5–37.5 °C throughout the recording. The transplanted site in the cortex was found under a water immersion objective (×20, 1.0 NA) according to the blood vessels previously recorded during transplantation.

The red calcium indicator Rhod-2 acetoxymethyl ester (Rhod-2AM, Invitrogen) was used for labeling astrocytes, as previously described (Takano et al. 2006; Thrane et al. 2012). In brief, rhod-2AM was dissolved in dimethylsulfoxide (DMSO) with 20% pluronic F-127 and diluted with the normal ACSF to a final concentration of ~0.5 mM, and then loaded onto exposed cortex for 10 min, followed by a 30-min wash with ACSF. After that, ACSF containing 1% agarose was applied on the top of the craniotomy to reduce brain pulsation-induced motion artifacts. Two-photon imaging was performed with a custom-designed two-photon microscope system based on 12 kHz resonant scanner (model “LotosScan 1.0”, Suzhou Institute of Biomedical Engineering and Technology). Two-photon excitation light was delivered by a mode-locked Ti:Sa laser (model “Mai-Tai DeepSee”, Spectra Physics), and a ×40/0.8 NA water-immersion objective (Nikon) was used for imaging. Full-frame images with 600 × 600 pixels were acquired at 40 Hz by custom-written software based on LabVIEW (National Instruments). The excitation laser wavelength was operated at 825 nm for imaging of Rhod-2-labeled astrocytes but at 920 nm for imaging the EGFP labeling. This two-channel detection was achieved using a 570-nm dichroic mirror. The imaged depth was in the range of 50–500 μm and the average power delivered to the brain was adjusted to 30–70 mW (depending on the depth). For hindlimb stimulation, electrical stimulation (duration 1 s, intensity 0.6–1 mA) was delivered to the hindpaws through two 30-gauge needles connected to an isolated pulse stimulator (A-M Systems).

Dextran Labeling and Two-Photon Imaging

We labeled and imaged blood vessels as previously described (Bardehle et al. 2013). In brief, anesthetized mice were injected intravenously (tail vein) with 50 μL of a solution (10 mg/mL) of

Texas Red-conjugated dextran (70 kDa; Molecular Probes D1864) to label blood vessels. Head-bar fixed, anesthetized, and craniotomized mice were placed on a heated stage, and imaging was performed with a custom-designed two-photon microscope system equipped with 12 kHz resonant scanner (model "LotosScan 1.0", Suzhou Institute of Biomedical Engineering and Technology), a water immersion objective (×40, 0.8 NA) and 570-nm dichroic mirror. The excitation laser wavelength was operated at 825 nm for imaging of Dextran-labeled blood vessels but at 920 nm for imaging the EGFP labeling.

Tissue Fixation and Vibratome Sectioning for Electron Microscopy

The brains of engrafted FVB/N mice were fixed and sectioned as described previously (Wilke et al. 2013). Briefly, mice were anesthetized with sodium pentobarbital and then perfused with Ringer's solution containing 0.02% heparin, followed by 2.5% electron microscopy grade glutaraldehyde (Sigma) and 4.0% paraformaldehyde (Sigma) in 0.1 M PBS (pH 7.2). The brain was then dissected free and postfixed in the same fixative solution at 4 °C for 7 h. After fixation, the tissue of interest was cut into thick (100 μm) sections using a vibratome. These sections were temporarily mounted in PBS under a coverslip in imaging chambers built using Parafilm spacers on a glass slide.

Near-Infrared Branding

We applied the previously-established procedure (Bishop et al. 2011) to make NIRB marks using the commercial two-photon microscope (Zeiss LSM780NLO), equipped with a mode-locked Ti:Sa laser (model "Mai-Tai DeepSee", Spectra Physics). Briefly, we created fiducial branding marks using the laser wavelength of 820 nm and using line scans (pixel dwell time 2–20 μs). The laser intensity delivered to the target region was ~300 mW. We usually burned two boxes, a large one (about 100 μm × 100 μm) containing almost the entire processes of engrafted astrocyte of interest, and a small one (about 10 μm × 10 μm) containing the site of interest where the process element and the presynaptic structure were colocalized. Images of NIRB marks were obtained from two-photon or confocal image stacks before and after marking.

Staining for Electronic Microscope and Resin Embedding

Slices were stained for electronic microscope (EM) imaging as previously reported (Wilke et al. 2013). In brief, slices were washed in 0.1 M cacodylate buffer for 2 h at 4 °C and placed in double-distilled water (ddH_2O) containing 2% OsO_4 for 2 h at room temperature. Slices were washed in ddH_2O at room temperature six times with 5 min for each time, before being placed in a filtered solution of 1% thiocarbohydrazide (EMS) in ddH_2O for 25 min to allow additional osmium staining. Slices were washed six times in ddH_2O and then placed in 2% OsO_4/1.5% potassium ferrocyanide for an additional 1 h at room temperature. Finally, slices were washed three times in ddH_2O and placed in 2% aqueous uranyl acetate at 4 °C overnight.

Slices were then washed six times in ddH_2O and then dehydrated in a series of acetone solutions (50%, 70%, 80%, 90%, 95%, 99%, 100%, 100% × 3; 5 min for each, on ice). We next placed slices in 100% propylene oxide for 10 min on ice. Slices were then gradually equilibrated with Spurr embedding resin by placing in 25% Spurr resin/propylene oxide for 6 h, 50% Spurr resin/propylene oxide overnight, 75% Spurr resin/propylene oxide for 12 h, and 100% Spurr resin overnight. Afterwards, slices were flat mounted in fresh 100% Spurr and placed in a 70 °C oven for 48 h to allow Spurr polymerization and to complete the embedding procedure.

Focused Ion Beam Scanning Electron Microscopy Imaging

Focused ion beam scanning electron microscopy (FIBSEM) imaging of our samples was performed as previously reported (Li et al. 2013; Maco et al. 2014). Briefly, images of the final block in the light microscope (×20 objective) were taken to ensure that it shows the NIRB marks inside the tissue, relative to the block edge, steps cut on either side. The block was carefully trimmed to expose the NIRB for FIBSEM imaging with Helios NanoLab 600i (FEI). A layer of platinum 1.5 μm thick was deposited on a surface perpendicular to the block face to be imaged. The block face was imaged using an electron beam with an acceleration voltage of 3 keV, a current of 2.75 nA, and a dwell time of 15 μs/pixel. After the block face was imaged, gallium ion beam with an acceleration voltage of 30 keV and a current of 2.5 nA was used to remove the 20-nm-thick superficial layer from the block face for the next round of imaging and milling. After the entire volume was acquired, the host and engrafted astrocyte processes of interest were traced and annotated with the ilastik program as the established criteria (Maco et al. 2014). The final 3D model can then be exported to 3D modeling software (Autodesk 3ds Max) for measurements and rendering.

Data Analysis

Ca^{2+} signals in astrocytes were expressed as relative fluorescence changes ($\Delta f/f$), corresponding to the mean fluorescence from all pixels within specified regions of interest, as described previously (Chen et al. 2011, 2012, 2013). Student's *t* tests were used to assess the significance of differences of branching point numbers, amplitude and latency of Ca^{2+} signals, A2B5/glial fibrillary acidic protein (GFAP) expression ratios and astrocyte/neuron differentiation ratios between experimental groups. Mann–Whitney *U* test was used to determine significance of differences of nAchR expression ratios between different time points after astrocyte precursor transplantation. Normal distributions were checked before all the tests. Statistical analyses were performed using SPSS (SPSS Inc.). $P < 0.05$ was considered as statistically significant.

Results

Engrafted Astrocytes are Morphologically Integrated into the Adult Neocortex

To explore the in vivo functional status of engrafted astrocytes, we transplanted glial precursor cells derived from NSCs into the somatosensory cortex of adult mice (2–4 months old) (Fig. 1*A*). We obtained NSCs from embryonic day 14.5 to 15.5 $EGFP^+$ FVB/N mice (Fig. 1*B*). After treatment with medium containing CNTF and FBS for 2 days, the majority of the cells (90%) differentiated from NSCs were immunoreactive for A2B5 (Fig. 1*C*,*D*), a marker for glial precursor cells (Mi and Barres 1999; Barberi et al. 2003; Krencik et al. 2011; Jiang et al. 2013). These cells were used for the following transplantation experiments. Over another 10-day culture in the presence of FBS in vitro, 86% of the cells were identified as astrocytes by GFAP immunoreactivity (Fig. 1*E*,*F*). Confocal imaging revealed that these astrocytes showed Ca^{2+} signals in response to ATP

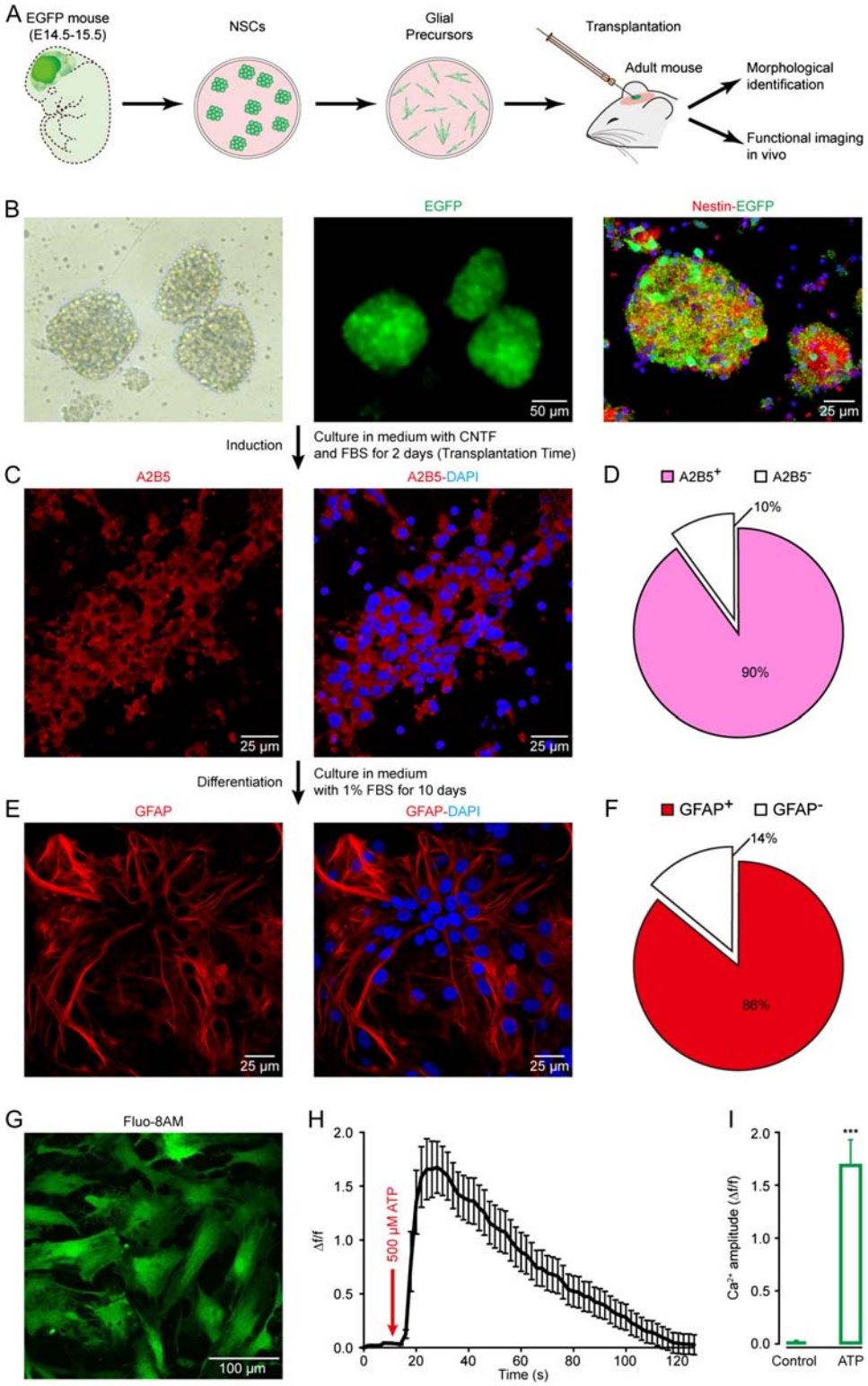

Figure 1. The identity of glial precursor cells derived from embryonic NSCs. (*A*) Experimental procedure for NSC isolation, glial precursor cell induction, cell transplantation, morphological and functional identification after transplantation. (*B*) Neurospheres, EGFP positive (green), formed by dissociated NSCs 4–5 days after being isolated and cultured. Immunolabeling for nestin (red) and EGFP. (*C*) Immunolabeling of cultured mouse glial precursor cells 2 days after being cultured in medium with CNTF and FBS. Immunostaining for A2B5 (red) and DAPI (blue). (*D*) Pie chart showing the fractions of A2B5-positive and negative cells. $n = 791$ cells in 7 fields of view. (*E*) Immunolabeling of cultured astrocytes 10 days after being cultured in medium with FBS. Immunostaining for GFAP (red) and DAPI. (*F*) Pie chart showing the fractions of GFAP-positive and -negative cells. $n = 757$ cells in 7 fields of view. (*G*) Representative confocal image of cultured astrocytes derived from NSCs labeled with fluo-8AM (green). (*H*) Ca^{2+} signals evoked by 500 μM ATP in the derived astrocytes ($n = 20$). (*I*) Bar graphs illustrate astrocytic Ca^{2+} amplitude ($\Delta f/f$) without (control) or with ATP ($n = 20$). Error bars show SEM. Student's *t* test, ***$P < 0.001$ versus the control.

(Fig. 1G–I), typical for functional astrocytes (Salter and Hicks 1995). Therefore, these glial precursor cells can mainly differentiate into astrocytes under the in vitro conditions.

We next tested whether the glial precursor cells could develop into astrocytes in vivo, and analyzed the survival and morphological profiles of the differentiated cells in the cortex over 4–60 weeks after transplantation. We found that all of the transplanted mice displayed robust survival of engrafted cells at all of the observed time points, and no sign of tumor formation was observed (Fig. 2A–E and Supplementary Fig. 1A–F). We found a range of 400–700 engrafted astrocytes (about 1% of all engrafted glial precursors) at different time points after transplantation (Supplementary Fig. 1G), comparable to the previous work (Sekiya et al. 2015). The vast majority of the surviving cells (83 ± 3% of 187 cells from 10 sections in 5 mice) were differentiated into astrocytes, identified by the expression of GFAP/EGFP/DAPI, whereas a small fraction (13 ± 4% of 133 cells from 6 sections in 5 mice) corresponded to the identity of neurons (Supplementary Fig. 2A–D). The engrafted astrocytes were also positive for connexin 30 (CX30) (Supplementary Fig. 3A,B), a major astrocytic gap junction protein (Kunzelmann et al. 1999), and D-serine (Supplementary Fig. 3C,D), a gliotransmitter (Schell et al. 1995). We also detected the expression of Kir4.1 (inwardly rectifying K^+ channels; Supplementary Fig. 4) and GLAST (glutamate/aspartate transporter; Supplementary Fig. 5) in the engrafted astrocytes, indicating that these cells have a potential ability to maintain homeostatic extracellular environments, including buffering extracellular K^+ and uptaking extracellular glutamate. Furthermore, similar to the adult mouse astrocytes that express almost no group I metabotropic glutamate receptors (mGluRs, mGluR5, and mGluR1) (Sun et al. 2013), we observed that at post-transplantation week 12, mGluR5 was undetectable in the engrafted astrocytes (n = 10 sections from 4 mice; 212 cells), whereas mGluR1 was sparsely expressed in only 13% of these cells (n = 5 sections from 4 mice; 103 cells) (Supplementary Fig. 6A–D). The morphological observation revealed that the engrafted astrocytes were clearly intermingled with host networks and evenly distributed along the injection sites in the cortical layers (Fig. 2A–E). At 12 weeks after transplantation, the engrafted astrocytes substantially developed dense and intricate processes, with a dramatically increased number of processes in comparison with that at 4 or 8 weeks, as quantified by the number of defined branching points (Fig. 2F and Supplementary Fig. 1F). The complexity and number of processes appeared to be largely stable over 60 weeks and closely matched the level of their host astrocytes (Fig. 2F). In vivo two-photon imaging revealed that the engrafted astrocytes extensively extended processes and established endfeet along the blood vessel walls (Fig. 2G–I), indicative of a role in cerebral microcirculation control (Takano et al. 2006; Iadecola and Nedergaard 2007). These results suggest that transplanted astrocytes are able to survive for at least 60 weeks and acquire characteristic molecular and morphological features of mature cortical astrocytes. It should be noted that, according to the previous work showing that cell fusion between transplanted and host cells specifically involves neurons (Brilli et al. 2013), it is unlikely that GFP-positive astrocytes observed here are due to fusion of engrafted cells with host astrocytes. Rather, the observed transplanted astrocytes are able to survive independently in the host cortex.

In addition, the transplanted cortical areas exhibited strong GFAP (Supplementary Fig. 7) and Iba1 (Ionized calcium binding adaptor molecule 1, a marker for activated microglia) (Supplementary Fig. 8) expression, while their contralateral hemispheres had weak or no expression. This suggests that the cell injection/engraftment produces reactive astrocytosis and microgliosis. A similar result has been already observed in the previous studies (Han et al. 2013; Chen et al. 2015). The traditional view is that reactive astrocytes have detrimental roles, for example, contributing to the formation of a glial scar (Silver and Miller 2004). However, recent evidence suggests that the reactive astrocytes can lead to a number of beneficial effects on the local environment (Lukovic et al. 2015).

Engrafted Astrocytes Respond with Ca^{2+} Signals to Sensory Stimulation

To test whether transplanted astrocytes could respond to sensory stimulation, like their host counterparts, we used two-photon imaging to monitor astrocytic Ca^{2+} dynamics in vivo. The transplanted region of somatosensory cortex containing EGFP-labeled astrocytes was bulk-loaded with the red Ca^{2+}-sensitive dye Rhod-2AM (Fig. 3A), an indicator that specifically labels astrocytes according to the previous studies (Takano et al. 2006; Schulz et al. 2012; Thrane et al. 2012). The engrafted astrocytes were colabeled with Rhod-2 and EGFP, whereas the nearby host astrocytes were labeled with Rhod-2 only, enabling a comparison of their response profiles in the same preparations (Fig. 3B). Figure 3B,C shows an example of such recordings at 12 weeks after transplantation, in which two engrafted (green) and one host (red) astrocytes reliably exhibited robust Ca^{2+} transients in their cell bodies and processes during every trial of electrical stimulation of the hindlimb. The somatic Ca^{2+} transients displayed a slow time course, often lasting for more than 10 s, in agreement with the previous observations that were done also in cortical astrocytes in vivo (Wang et al. 2006; Schummers et al. 2008). Moreover, these stimulation-evoked astrocytic Ca^{2+} responses started to appear at 12 weeks after transplantation but not at the time points before 8 weeks (Fig. 3D). At 12 weeks after transplantation, we found about 67% (67 ± 6%; n = 5 mice) of engrafted astrocytes responding to hindlimb stimulation, comparable to that of host astrocytes (69 ± 13%; n = 8 mice). Quantitative analysis of the cell body's response amplitude and latency revealed that sensory-evoked Ca^{2+} responses in these engrafted astrocytes remained stable for more than 25 weeks and showed comparable profiles to their corresponding host counterparts (Fig. 3D,E). In addition, we occasionally observed spontaneous Ca^{2+} activity in the engrafted astrocytes as well as in the host cells (engrafted astrocytes: 0.8 ± 0.1 $\Delta f/f$ versus host astrocytes: 0.9 ± 0.1 $\Delta f/f$; n = 19 cells for either group, P = 0.35; Supplementary Fig. 9A–C). These results indicate that embryonic NSC-derived astrocytes transplanted into the adult sensory cortex can manifest a functional phenotype that may contribute to executing sensory information processing, similar to genuine cortical astrocytes (Wang et al. 2006; Schummers et al. 2008; Ghosh et al. 2013).

nAchRs are Required for Sensory-Evoked Ca^{2+} Response in Engrafted Astrocytes

Previous studies have reported that the same type of electrical stimulation to the hindlimb used here produces cortical responses through the activation of cholinergic afferents from the basal forebrain (Wenk 1997; Seigneur et al. 2006; Letzkus et al. 2011). Ample evidence also indicates the expression of nAChR subunit α7 in astrocytes (Sharma and Vijayaraghavan 2001; Duffy et al. 2011; Shen and Yakel 2012; Wang et al. 2013), which might be required for mediating Ca^{2+} response in astrocytes (Sharma and Vijayaraghavan 2001) during this

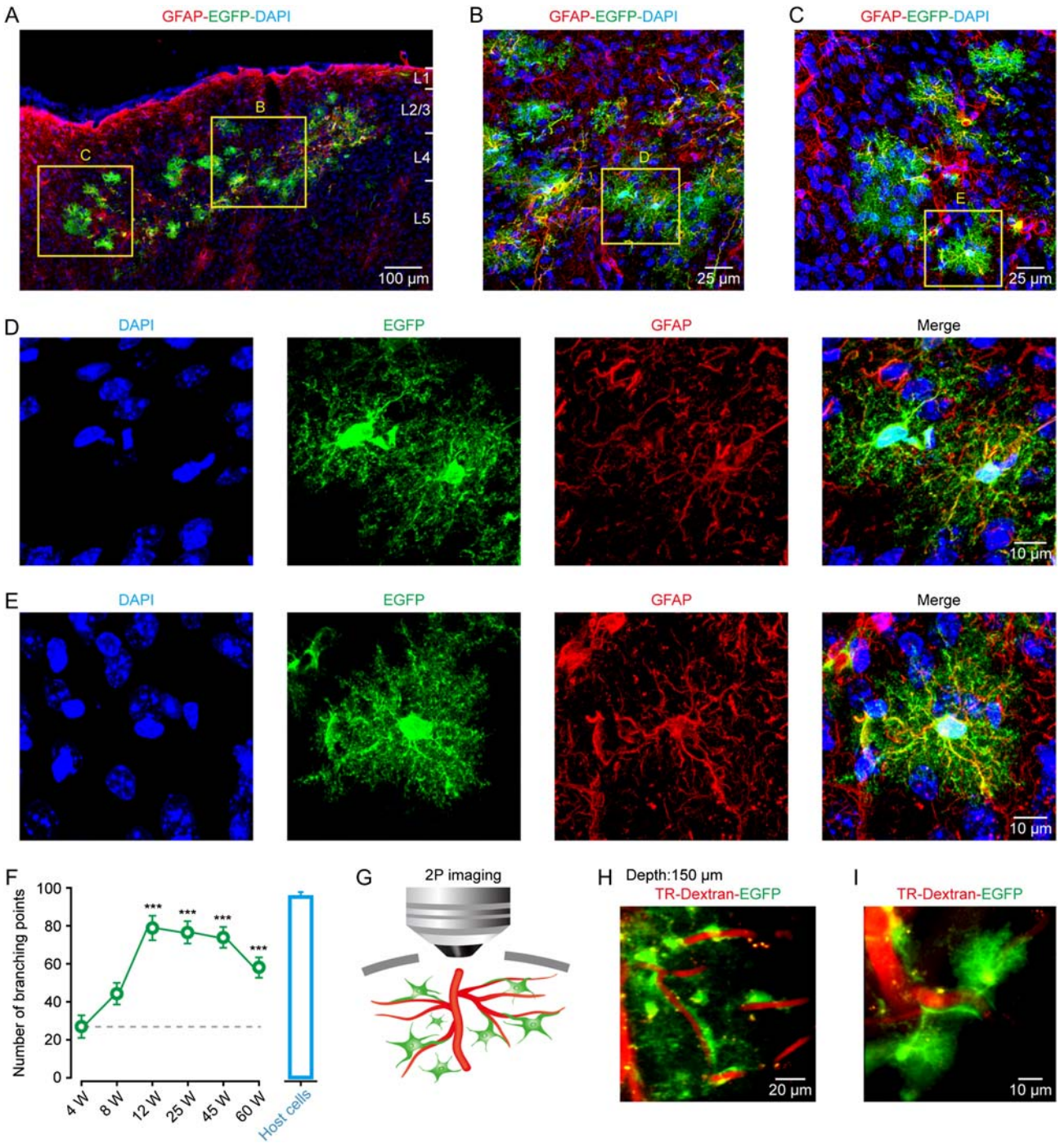

Figure 2. Engrafted astrocytes are morphologically integrated into the adult mouse cortex and survive for at least 60 weeks. (*A*) Representative image of engrafted astrocytes in a cortical region at 12 weeks after transplantation. Engrafted astrocytes, positive for EGFP/GFAP, were distributed in different cortical layers. DAPI was used to stain nuclei throughout the study.(*B–E*) Higher magnification of regions from panel *A* showing the complex fine structures of engrafted astrocytes ($EGFP^+$). (*F*) Summary of the number of processes of engrafted astrocytes at different weeks (W) after transplantation (green points), and of their host astrocytes (host cells, blue bar graph). The host cells are those GFP-negative but GFAP-positive cells from the same preparations. The number of processes is quantified by the defined branching points. $n = 20–21$ cells from 4 to 9 mice for each group; $^{***}P < 0.001$ versus 4 W, Student's *t* test. (*G*) Cartoon depicting the relative position between the processes of engrafted astrocytes and blood vessels under in vivo two-photon imaging setup. (*H*, *I*) Representative images of engrafted astrocytes ($EGFP^+$) wrapping and making contacts with blood vessels 12 weeks after transplantation. The vasculature was visualized using Texas Red-dextran (TR-Dextran). The depth from pial surface of the imaging is 150 μm.

stimulation. Therefore, we performed immunohistochemistry to examine the expression of α7 nAChRs in both engrafted and host astrocytes and to clarify their relative locations with presynaptic cholinergic terminals labeled by choline acetyltransferase (ChAT). Figure 4A–C shows an example of engrafted cortical astrocytes stained with EGFP/ChAT/α7 nAChR at 12 weeks after transplantation. According to EGFP labeling, the cell showed complex processes with extensive ramifications, a typical morphology of mature astrocytes (Fig. 4A and Supplementary Fig. 10A). The nAChRs were punctate staining

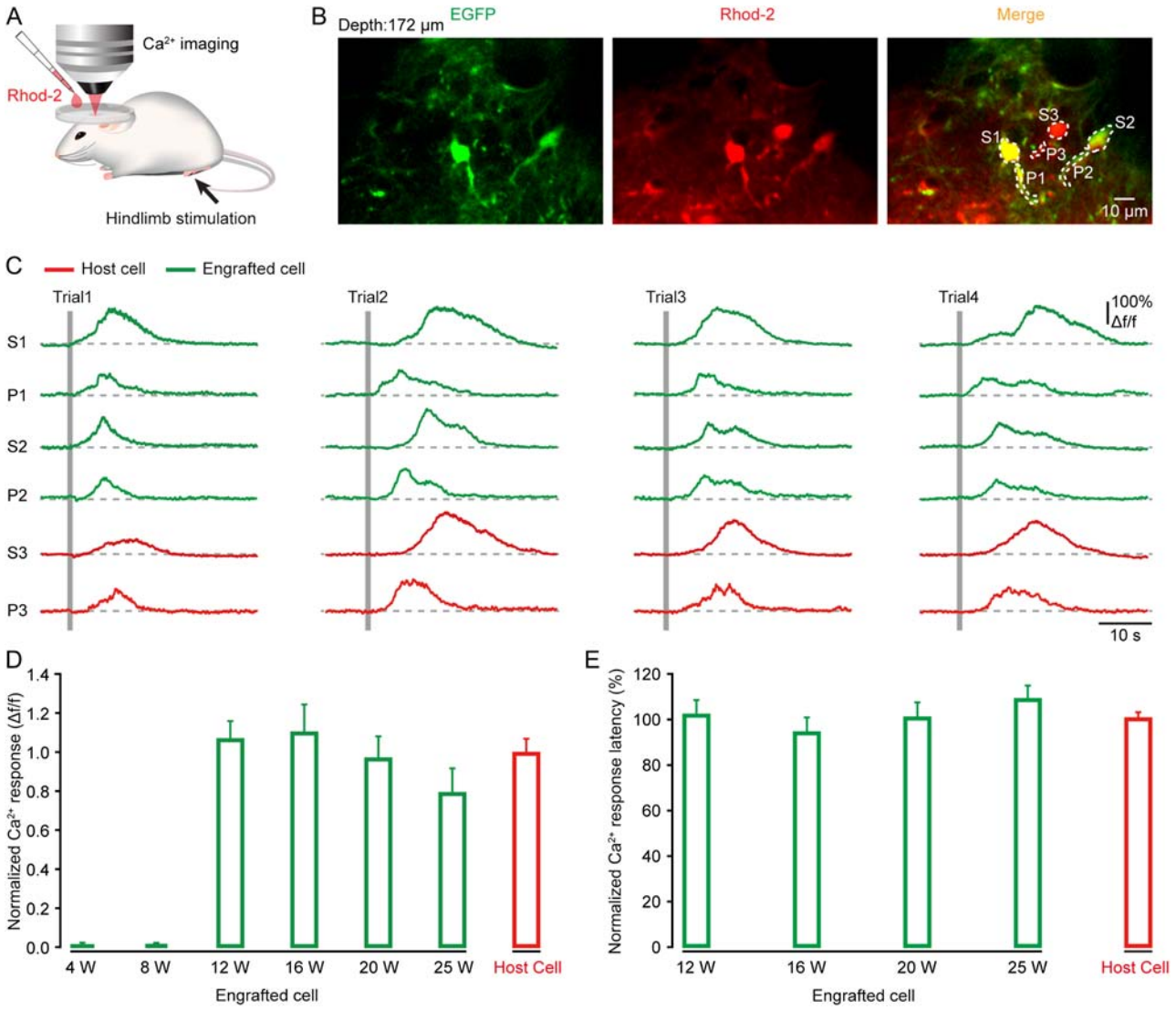

Figure 3. Sensory stimulation induces Ca^{2+} signals in engrafted astrocytes in the adult somatosensory cortex. (*A*) Schematic of the experimental procedure. Astrocytes were bulk loaded with Rhod-2AM by surface application. Electrical stimulation (duration 1 s, intensity 0.6–1 mA) was delivered to the hindlimb. (*B*) Two-photon image of engrafted ($EGFP^+$ and $Rhod\text{-}2^+$) and host ($Rhod\text{-}2^+$) astrocytes in the somatosensory cortex. Both somata (S) and processes (P) of astrocytes were observed. Two-photon imaging depth is 172 μm. (*C*) Ca^{2+} signals ($\Delta f/f$) in engrafted (green) and host (red) astrocytes outlined in panel *B* during hindlimb stimulation (indicated by gray bars; 1 s duration and 0.6 mA intensity). Ca^{2+} responses are shown from both somata (S) and processes (P). (*D*, *E*) Summary of the amplitude and latency of Ca^{2+} responses in engrafted astrocytes (green) at different weeks after transplantation (n = 11–35 cells from 3 to 5 mice for each time point), and in their host astrocytes (red, n = 64 cells from 8 mice). Each value was normalized to the mean value of the host group.

and dispersed along EGFP-labeled processes. Notably, nAChR puncta were often located next to ChAT-positive structures, indicating that they probably formed synapse-like contacts with cholinergic presynaptic elements (the same observation was seen in 30 cells from 16 sections in 9 mice; Fig. 4*B*,*C*). In support of this, nAChR puncta along EGFP-positive processes were also often found to face small enlargements labeled with synaptophysin (syn), a synaptic vesicle marker (n = 32 cells, 15 sections from 10 mice; Fig. 4*D*–*F* and Supplementary Fig. 10*B*). Puncta of nAchR were also observed independent of GFP-positive glial processes. These other structures may be host astrocytes or neurons, which were eGFP negative (Panatier et al. 2011). Overall, we found that after post-transplantation week 12, approximately 50% of the engrafted astrocytes expressed α7 nAChRs, significantly higher than that before 8 weeks but comparable to the number in mature host astrocytes (Fig. 4*G*).

To further determine whether sensory stimulation-evoked Ca^{2+} signals in engrafted astrocytes were cholinergic input driven and nAChR mediated, we locally applied the nAChR antagonist methyllycaconitine (MLA, 100 μM) using a glass pipette under visual guidance by two-photon imaging (Fig. 5*A*). We found that MLA completely abolished the Ca^{2+} responses to sensory stimulation in the engrafted astrocytes (n = 21 cells from 4 mice, $P < 0.001$ versus the control group), similar to the nearby host cells (n = 10 cells from 4 mice, $P < 0.001$ versus the control group) (Fig. 5*B*–*D*). Interestingly, a fraction of engrafted astrocytes (~20%) clearly showed Ca^{2+} responses to a local nicotine application (100 μM) (n = 19 cells; Supplementary Fig. 9*D*,*E*) even at 4 weeks after transplantation, being much earlier than the occurrence of sensory-evoked Ca^{2+} responses (Fig. 3*D*). This indicates the presence of nAChRs already at 4 weeks in a subpopulation of engrafted astrocytes (also see Fig. 4*G*) but a lack of

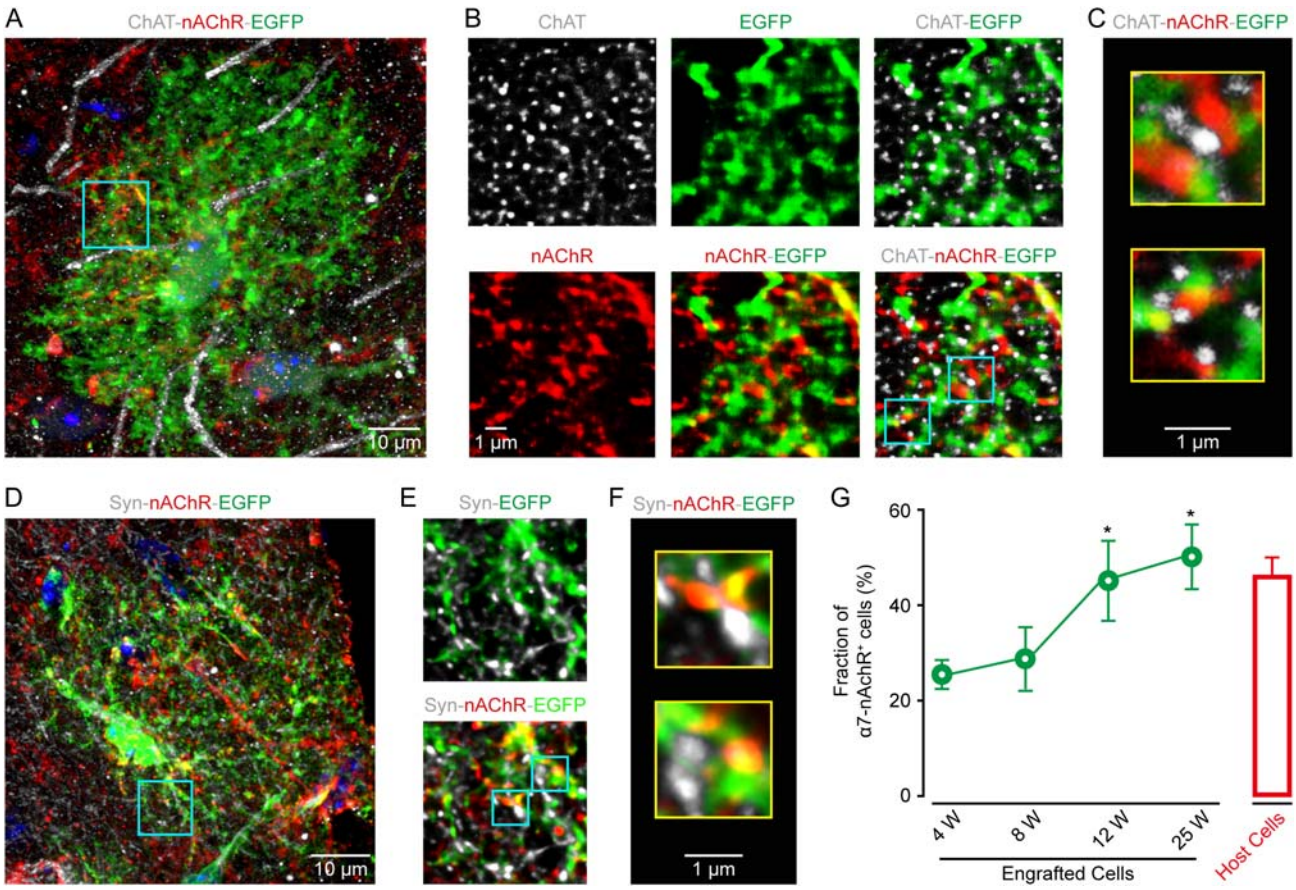

Figure 4. Engrafted astrocytes express nicotinic acetylcholine receptors. (*A*) Immunostaining image of EGFP (green) for engrafted astrocytes, ChAT (gray) for cholinergic structures, and nAChR α7 (red) in the somatosensory cortex at 12 weeks after transplantation. (*B*) High magnification of the region outlined in panel *A*. (*C*) Higher magnification of two regions outlined in panel *B*, showing engrafted astrocytic processes (EGFP+), often expressing nAchRs and next to presynaptic cholinergic puncta (ChAT+). (*D*) Confocal image of synaptophysin (syn, gray), nAchR (red), and EGFP (green) in a transplanted cortical region at post-transplantation week 12. (*E*) High magnification of the expression of Syn, EGFP and α7 of the region outlined in panel *D*. (*F*) Higher magnification of two regions outlined in panel *E*. nAchR labeling decorates engrafted astrocytic processes ($EGFP^+$), often facing syn-labeled (Syn^+) presynaptic elements. (*G*) Fraction of $nAchR^+$ engrafted astrocytes (green) at different weeks after transplantation (n = 4–7 sections, 41–150 cells from 4 mice for each group), and of their host astrocytes (red, n = 4 sections, 72 cells). Mann–Whitney U test, $^*P < 0.05$ versus 8 W.

functional connections between these cells and the host cholinergic terminals.

Our immunostaining data showed that approximately 50% of astrocytes expressed α7 nAChRs (Fig. 4*G*), which cannot explain the complete blockade of the hindlimb stimulation-induced Ca^{2+} signals by MLA in all the responding astrocytes (67 ± 6% for engrafted astrocytes and 69 ± 13% for host astrocytes). There might be another mechanism, for example, gap-junction-mediated glia-to-glia communication (Kuga et al. 2011), that also contributes to the hindlimb stimulation-induced astrocytic activation. To test this possibility, we applied the gap junction blocker carbenoxolone (CBX) to host astrocytes and found that CBX reduced the fraction of responding cell by ~10% (Supplementary Fig. 11). Therefore, these results suggest that the nAChR-mediated activation plays a major role, while the gap junction plays a minor role in the hindlimb stimulation-evoked astrocytic responses through glia-to-glia communication.

In addition, previous studies have observed that a startle response can produce astrocytic Ca^{2+} signals through norepinephrine-mediated activation of α-adrenergic receptors in the somatosensory (Bekar et al. 2008) and the visual cortex (Paukert et al. 2014). However, in our experiments that were performed in both anesthetized and awake states, we found that the α1-adrenergic antagonist, phentolamine, had no effect on the hindlimb stimulation-evoked Ca^{2+} signals in host astrocytes (Supplementary Fig. 12). The lack of norepinephrine contribution in our study could be due to a different stimulation intensity used here as compared with the previous study (Bekar et al. 2008).

Engrafted Astrocytes Establish Synapse-Like Contacts with the Basal Forebrain Sholinergic Axonal Terminals

We next investigated whether the engrafted astrocytes could indeed establish synaptic contacts with the host cholinergic axonal terminals, originating from the basal forebrain (Wenk 1997), by observing their ultrastructural features using electron microscopy. To this end, we devised an experiment to first label the basal forebrain cholinergic projections in the cortex by injecting the red dextran dye mini-ruby into the nucleus basalis of Meynert (Fig. 6*A* and see the injection site in Supplementary Fig. 13). Figure 6*B–G* shows examples in the transplanted cortex at post-transplantation week 12 for mini-ruby labeling together with the immunostaining of EGFP/DAPI/nAChR (Fig. 6*B–D* and Supplementary Fig. 14*A*) or EGFP/DAPI/ChAT (Fig. 6*E–G* and

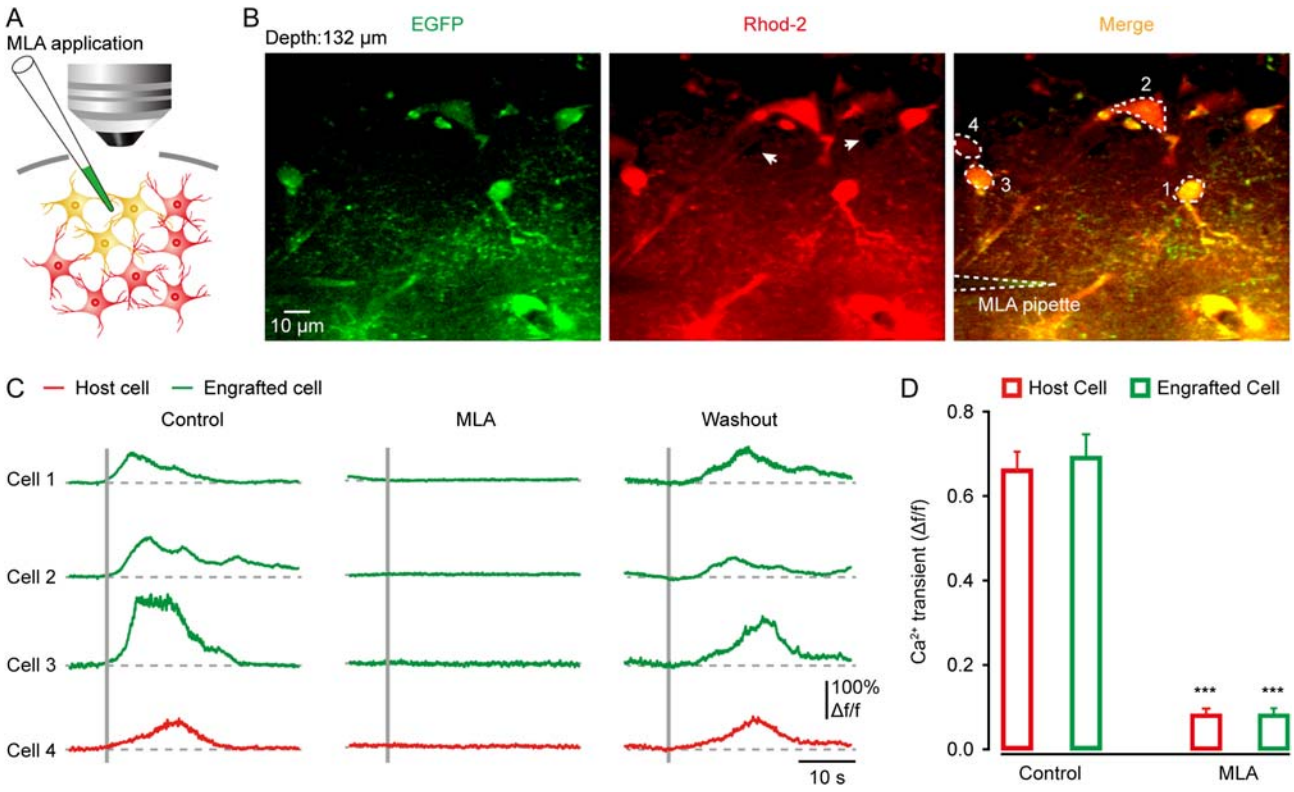

Figure 5. Sensory-evoked Ca^{2+} response in engrafted astrocytes requires the activation of nicotinic receptors. (*A*) Schematic of the experimental procedure for pharmacological manipulation. (*B*) Two-photon image of engrafted ($EGFP^{+}$/Rhod-2^{+}) and host astrocytes (Rhod-2^{+}) in the somatosensory cortex at 12 weeks after transplantation. White-dashed lines indicate MLA delivery pipette. White arrows point to the unlabeled neurons appearing as dark holes. Two-photon imaging depth is 132 μm. (*C*) Sensory-evoked Ca^{2+} signals before, during, and after MLA application, in engrafted (green) and host (red) astrocytes outlined in panel *B*. (*D*) Summary of the response amplitude in the engrafted ($n = 21$ cells from 4 mice for each group) and host astrocytes ($n = 10$ cells), with or without MLA. Student's *t* test, ***$P < 0.001$ versus the control.

Supplementary Fig. 14*B*), in which mini-ruby-labeled punctate compartments were widely found in the cortex and overlapped with engrafted astrocytic processes stained by EGFP (Fig. 6*B*,*E*). Mini-ruby-labeled axonal terminals often appeared to be colocalized with ChAT-positive presynaptic elements ($n = 25$ cells, 8 sections from 4 mice) (Fig. 6*F*,*G*) and with nAChR-positive astrocytic sites ($n = 35$ cells, 11 sections from 6 mice) (Fig. 6*C*,*D*), indicating their identity of cholinergic afferents and the possible connections with astrocytes.

Next, we used a previously developed protocol, near-infrared branding (NIRB) (Bishop et al. 2011), to selectively mark an area containing possible synaptic contacts where EGFP- and mini-ruby-positive elements were juxtaposed, using a femtosecond pulsed titanium-sapphire laser under the guidance of two-photon imaging (Fig. 7*A*,*B*). These marks allowed for the re-identification and reconstruction of the target structures of interest using subsequently performed serial electron microscopy (Fig. 7*C*–*E*). We identified the astrocytic processes according to the following EM morphological features (Ventura and Harris 1999; Witcher et al. 2007): (1) their irregular shapes interdigitating among neuronal processes; (2) the presence of glycogen granules; (3) intermediate filament bundles, and (4) a relatively clear cytoplasm. In addition, before the NIRB using two-photon imaging, engrafted astrocytes could be readily identified from engrafted neurons based on their morphological profiles (e.g., see Fig. 2 and Supplementary Fig. 2). We excluded engrafted neurons for the branding. As in the examples shown in Figure 7*F*–*H* (also see examples for both engrafted and host astrocytes in Supplementary Fig. 15*A*–*F*), we observed that astrocytic processes established contacts with mini-ruby-labeled axonal terminals from the basal forebrain in two ways: first, tripartite synapses, in which astrocytic processes enwrapped synapses between presynaptic (e.g., red in Fig. 7*G* and Supplementary Fig. 15*A*,*E*) and postsynaptic sites (e.g., blue in Fig. 7*G*, pointed by arrows; Supplementary Fig. 15*A*,*E*); second, synapse-like structures, also observed previously (Jabs et al. 2005), which were formed directly between presynaptic terminals and astrocytic processes (e.g., see postsynaptic density-like structures in Fig. 7*G*, pointed by arrowheads). Overall, using this combined approach of optical and electron microscopy, we found nearly an equal number of these two types of contacts for both the engrafted ($n = 121$ synaptic contacts, 3 cells from 2 mice) and host astrocytes ($n = 106$ synaptic contacts, 3 cells from 2 mice; Fig. 7*I*,*J*).

Discussion

In this study, we show that glial precursor cells derived from mouse NSCs can mainly generate astrocytes under both in vitro and in vivo conditions, although these precursor cells used here are heterogeneous glial populations. Using this cell preparation for transplantation together with the use of a number of approaches including immunostaining analysis, in vivo two-photon Ca^{2+} imaging, pharmacological manipulations, fluorescent indicator labeling-based axon tracing and correlated light and electron microscopy, we provide the first in vivo demonstration for the functional integration of transplanted astrocytes into the adult neocortex. We find that, after

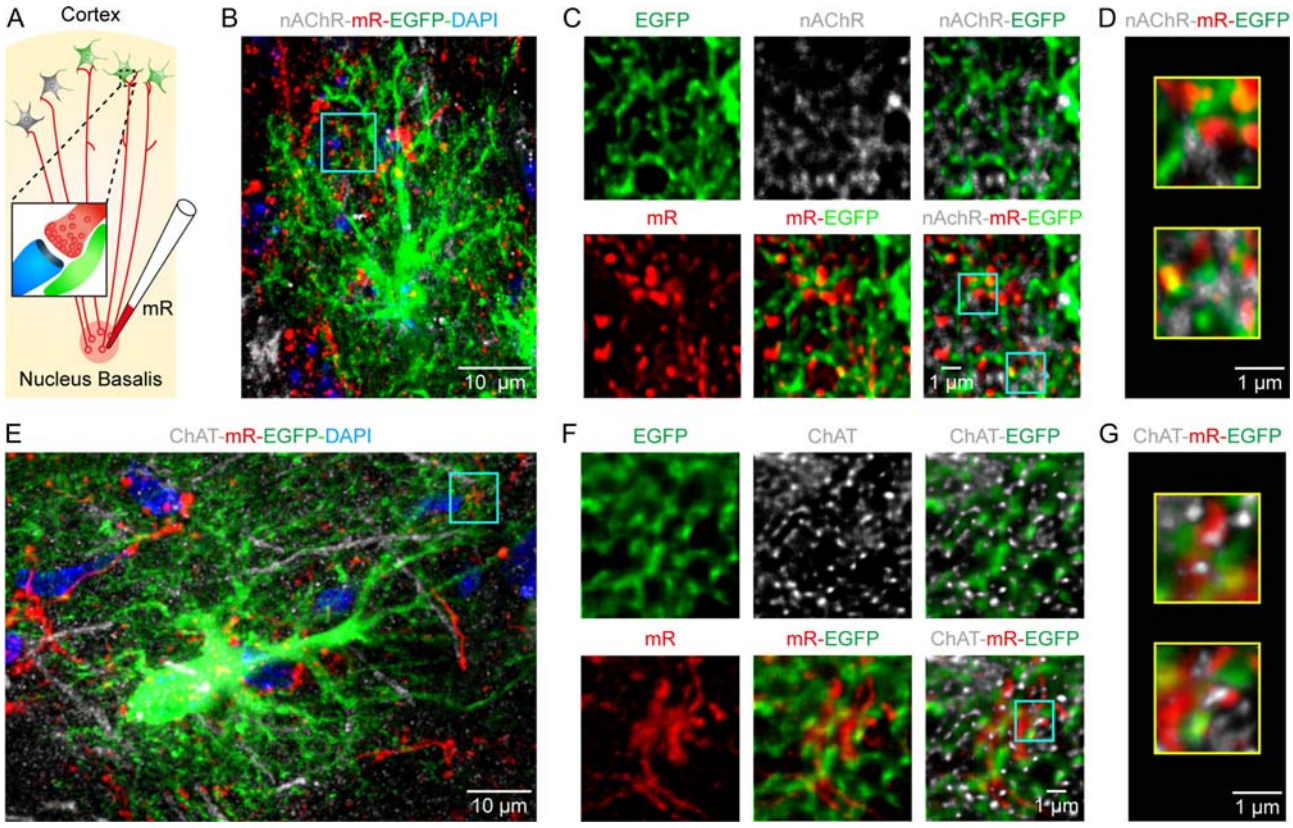

Figure 6. Light microscopic evidence for the formation of synapse-like contacts between engrafted astrocytes and basal forebrain cholinergic axonal terminals. (*A*) Experimental procedure for mini-ruby-based tracing of cholinergic projections from the nucleus basalis of Meynert to the cortex. Inset, possible tripartite synapse among the cholinergic axon (red), postsynaptic site (blue), and process of engrafted astrocyte (green). (*B*) Confocal image of an engrafted astrocyte ($EGFP^+$), nAChR expression, and mR^+ axons in the cortical region 12 weeks after transplantation. (*C*) High magnification of the region outlined in panel *B*. (*D*) Higher magnification of two regions outlined in panel *C*. nAchR labeling of engrafted astrocytic processes ($EGFP^+$), which are often next to presynaptic puncta (mR^+). (*E*–*G*) The same arrangement as in panels *B*–*D*, showing an $EGFP^+$ engrafted astrocyte, cholinergic structures ($ChAT^+$), and mR^+ axons in the cortical region at 12 weeks after transplantation.

transplantation into the mouse sensory cortex, the engrafted astrocytes exhibit the important characteristics that are similar to their host counterparts, including molecular, morphological, and most importantly, functional phenotypes namely robust Ca^{2+} response to sensory stimulation. The sensory-evoked Ca^{2+} responses are attributed to the functional expression of nAChRs and the targeted establishment of synapse-like contacts with cholinergic neuronal afferents in the host circuits, as assessed by both morphological analyses and in vivo cellular imaging in combination of pharmacological blockage of nAChRs.

Astrocytes are active participants essential for a wide variety of physiological processes in the mammalian brain (Araque et al. 1999; Volterra and Meldolesi 2005; Halassa and Haydon 2010; Nedergaard and Verkhratsky 2012). Of particular importance is that astrocytes are extensively considered to be integrated communication elements together with neurons and blood vessels for executing central functions of the brain, namely information processing through Ca^{2+} excitability-dependent gliotransmitter release (Wang et al. 2009; Lopez-Hidalgo and Schummers 2014; Volterra et al. 2014). In addition, many brain diseases and also aging processes are known to involve astrocyte dysfunctions (Seifert et al. 2006; Kuchibhotla et al. 2009; Sofroniew and Vinters 2010; Rodriguez-Arellano et al. 2016). Therefore, brain remodeling involving cell replacement-based strategy requires consideration of the restoration of both neuron and astrocyte functions. In support of this notion, multiple lines of experimental evidence indicate that astrocyte or its precursor transplantation improves brain or spinal cord functions and even changes the related behavioral ability (Smith and Silver 1988; Muller and Best 1989; Lepore et al. 2008; Chintawar et al. 2009; Davies et al. 2011; Han et al. 2013; Jiang et al. 2013; Chen et al. 2015). These behaviorally-relevant outcomes may be due to the functional integration of transplanted astrocytes into the host circuits. However, existing data from these studies for supporting their integration were mainly obtained from molecular and morphological experiments. Functional experiments, including voltage-clamp recordings and measurement of intracellular Ca^{2+} waves by the photolysis of caged Ca^{2+} procedure (Han et al. 2013; Jiang et al. 2013), performed in brain slice preparations can provide a confirmation only for the identity of astrocytes but not for the functional integration. So far, indirect evidence for the functional integration has been acquired from also in vitro experiments showing changes in neuronal activity by glia transplantation, for example, the enhancement of neuronal transmission and the emergence of synaptic plasticity in neurons (Han et al. 2013; Jiang et al. 2013). In the current study, we used in vivo two-photon imaging to directly monitor the functional status of engrafted astrocytes and showed their existence of Ca^{2+} signals, a major type of cellular responsiveness of astrocytes, in response to electrical stimulation of the

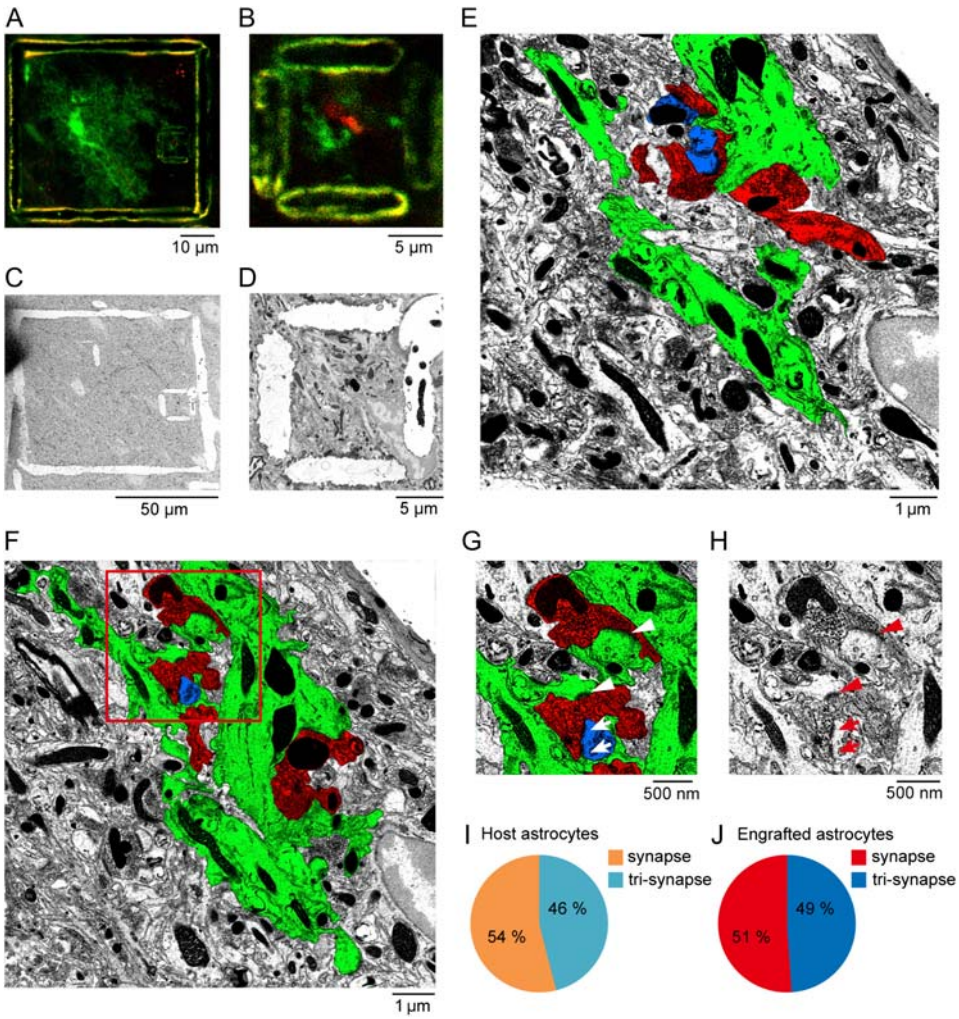

Figure 7. Electron microscopic evidence for the formation of synapse-like contacts between engrafted astrocytes and cholinergic axonal terminals. (*A*) Two-photon image of EGFP (green) positive engrafted astrocytes and mini-Ruby (red) positive axons projected from the nucleus basalis of Meynert in a cortical section, after NIRB. The large NIRB box outlines an entire engrafted astrocyte, while the small box outlines a juxtaposed site of the process of the engrafted astrocyte (green) with a mini-Ruby labeled axonal site (red). (*B*) High magnification of the target region outlined by the small NIRB box in panel *A*. (*C*) Low-power electron microscopic image of the target region after switching from thick sectioning to ultrathin sectioning. The NIRB markers can be readily observed. (*D*) High-power electron micrograph of the small NIRB box, the same as in panel *B*. (*E*) Ultrathin section of processes of engrafted astrocytes (green) and mini-Ruby labeled axon (red) outlined by the NIRB mark in panel *D*. False color image shows the processes of engrafted astrocytes in green, mR-labeled axons in red, and a postsynaptic structure of a host neuron in blue. (*F*) Another example of electron micrograph. (*G*) High magnification of the region outlined in *F*, showing both synaptic-like structures (arrowheads) and tripartite synapses among the processes of astrocyte (green), the mR^+ axon (red), and the postsynaptic site (blue) (arrows). (*H*) The actual EM image, corresponding to *G*. (*I*, *J*) Summary of the percentage of synaptic-like structures (synapse) or tripartite synapses (tri-synapse) formed between host astrocytes and neurons ($n = 106$ synaptic contacts, 3 cells from 2 mice), or between engrafted astrocytes and neurons ($n = 121$ synaptic contacts, 3 cells from 2 mice).

hindlimb. As sensory-evoked astrocytic Ca^{2+} responses require the information signal flow through certain functional neuron–glia circuits (Wang et al. 2006; Ghosh et al. 2013; Lopez-Hidalgo and Schummers 2014), these results represent, to the best of our knowledge, the first evidence for a functional incorporation of engrafted astrocytes into the adult mammalian brain and also for their involvement in sensory information processing. This in vivo validation of functional integration into the host brain is also supported by the morphological observations of expression of nAChRs and existence of synapse-like contacts with cholinergic neuronal afferents.

Astrocyte-based transplantation can produce different physiologically-related improvements for the functions of the central nervous system. In the spinal cord of a rat model of amyotrophic lateral sclerosis, focal transplantation of astrocytes extends survival and disease duration, reduces motor neuron loss, and slows down declines in behavioral performance (Lepore et al. 2008). When transplanted into the injured adult rat spinal cord, engrafted astrocytes from human glial precursors also promote significant behavioral recovery (Davies et al. 2011). An early study has reported that, in the visual cortex of adult cats, transplanted astrocytes re-induce ocular-dominance plasticity (Muller and Best 1989). More recently, two papers have shown that transplanted astrocyte derived from human glial progenitor cells in the brain can protect neurons and improve behavioral performance after global ischemic brain injury in rats (Jiang et al. 2013) or enhance both activity-dependent plasticity and learning ability in mice when engraftment is done into neonatal immunodeficient mice (Han et al. 2013). Unlike other studies that were done in neonatal immunodeficient mice (e.g. Han et al. 2013), our transplantation was performed in adult physiological brain. Thus, this work

provides a more suitable strategy for the treatment of neurological disorders or adult brain injuries. In addition, we used mouse-to-mouse transplantation instead of transplantation from human pluripotent stem cells or from human fetal tissues to the mouse brain (Han et al. 2013; Jiang et al. 2013; Chen et al. 2015), as cell transplantation using tissues from the same species is more relevant for clinical applications. Therefore, further experiments are needed to explore whether glia transplantation into the adult somatosensory cortex as demonstrated in this study indeed has any therapeutic relevance.

Classically, astrocytes have been suggested to interact with neuronal networks mainly through tripartite synapses that involve metabotropic glutamate receptor-mediated Ca^{2+} signals and their mediated gliotransmitter release (Araque et al. 1999; Chen et al. 2005; Eroglu and Barres 2010; Panatier et al. 2011). Recent work has doubted the existence of this well-established form of synaptic contact between astrocytes and neurons by showing the lack of expression of mGluR5 in the adult brain (Sun et al. 2013). Our results suggest that, similar to their host counterparts, engrafted astrocytes are able to develop numerous synapse-like structures as well as tripartite synapses in contact with the cholinergic projections in the host cortex, which possibly accounts for the sensory-evoked nAChR-mediated astrocytic Ca^{2+} signals observed here. Therefore, these findings have an extended implication in parallel to the aspect of glia transplantation. Namely, we identified a new form of tripartite synapse between astrocytes and cholinergic neuronal terminals in addition to their classical form involving glutamatergic transmission. Together, we provide strong support for the application of glial precursor transplantation to explore glia-related neural development in vivo.

Supplementary Material

Supplementary material can be found at: http://www.cercor.oxfordjournals.org/.

Funding

This study was supported by grants from the Nature Science Foundation of China (No. 91232721, 31400933, 31327901) and the National Basic Research Program of China ("973Program": 2015CB759500, 2014CB541600). X.C. is a junior fellow of the CAS Center for Excellence in Brain Science of the Chinese Academy of Sciences.

Notes

We thank J. Lou for assistance in composing figures, J. Zhang (the Center for Biological Imaging, Institute of Biophysics, Chinese Academy of Science) for technical support on focused ion beam scanning electron microscopy imaging, Dr Y. Hu (the Core Facilities of College of Life Sciences, Peking University) for technical assistance on electron microscopy sample preparation and data analysis, Dr T. Misgeld for advice on near-infrared branding experiments. *Conflict of Interest:* None declared.

References

Araque A, Parpura V, Sanzgiri RP, Haydon PG. 1999. Tripartite synapses: glia, the unacknowledged partner. Trends Neurosci. 22:208–215.

Barberi T, Klivenyi P, Calingasan NY, Lee H, Kawamata H, Loonam K, Perrier AL, Bruses J, Rubio ME, Topf N, et al. 2003. Neural subtype specification of fertilization and nuclear transfer embryonic stem cells and application in parkinsonian mice. Nat Biotechnol. 21:1200–1207.

Bardehle S, Kruger M, Buggenthin F, Schwausch J, Ninkovic J, Clevers H, Snippert HJ, Theis FJ, Meyer-Luehmann M, Bechmann I, et al. 2013. Live imaging of astrocyte responses to acute injury reveals selective juxtavascular proliferation. Nat Neurosci.16:580–586.

Bekar LK, He W, Nedergaard M. 2008. Locus coeruleus alpha-adrenergic-mediated activation of cortical astrocytes in vivo. Cereb Cortex. 18:2789–2795.

Bishop D, Nikic I, Brinkoetter M, Knecht S, Potz S, Kerschensteiner M, Misgeld T. 2011. Near-infrared branding efficiently correlates light and electron microscopy. Nat Methods. 8:568–570.

Brilli E, Reitano E, Conti L, Conforti P, Gulino R, Consalez GG, Cesana E, Smith A, Rossi F, Cattaneo E. 2013. Neural stem cells engrafted in the adult brain fuse with endogenous neurons. Stem Cells Dev. 22:538–547.

Chen H, Qian K, Chen W, Hu B, Blackbourn LW, Du Z, Ma L, Liu H, Knobel KM, Ayala M, et al. 2015. Human-derived neural progenitors functionally replace astrocytes in adult mice. J Clin Invest. 125:1033–1042.

Chen X, Leischner U, Rochefort NL, Nelken I, Konnerth A. 2011. Functional mapping of single spines in cortical neurons in vivo. Nature. 475:501–505.

Chen X, Leischner U, Varga Z, Jia H, Deca D, Rochefort NL, Konnerth A. 2012. LOTOS-based two-photon calcium imaging of dendritic spines in vivo. Nat Protoc. 7:1818–1829.

Chen X, Rochefort NL, Sakmann B, Konnerth A. 2013. Reactivation of the same synapses during spontaneous up states and sensory stimuli. Cell Rep. 4:31–39.

Chen X, Wang L, Zhou Y, Zheng LH, Zhou Z. 2005. "Kiss-and-run" glutamate secretion in cultured and freshly isolated rat hippocampal astrocytes. J Neurosci. 25:9236–9243.

Chintawar S, Hourez R, Ravella A, Gall D, Orduz D, Rai M, Bishop DP, Geuna S, Schiffmann SN, Pandolfo M. 2009. Grafting neural precursor cells promotes functional recovery in an SCA1 mouse model. J Neurosci. 29:13126–13135.

Davies SJ, Shih CH, Noble M, Mayer-Proschel M, Davies JE, Proschel C. 2011. Transplantation of specific human astrocytes promotes functional recovery after spinal cord injury. PLoS One. 6:e17328.

Duffy AM, Fitzgerald ML, Chan J, Robinson DC, Milner TA, Mackie K, Pickel VM. 2011. Acetylcholine alpha7 nicotinic and dopamine D2 receptors are targeted to many of the same postsynaptic dendrites and astrocytes in the rodent prefrontal cortex. Synapse. 65:1350–1367.

Eroglu C, Barres BA. 2010. Regulation of synaptic connectivity by glia. Nature. 468:223–231.

Ghosh A, Wyss MT, Weber B. 2013. Somatotopic astrocytic activity in the somatosensory cortex. Glia. 61:601–610.

Goldman SA, Nedergaard M, Windrem MS. 2012. Glial progenitor cell-based treatment and modeling of neurological disease. Science. 338:491–495.

Halassa MM, Haydon PG. 2010. Integrated brain circuits: astrocytic networks modulate neuronal activity and behavior. Annu Rev Physiol. 72:335–355.

Han X, Chen M, Wang F, Windrem M, Wang S, Shanz S, Xu Q, Oberheim NA, Bekar L, Betstadt S, et al. 2013. Forebrain engraftment by human glial progenitor cells enhances synaptic plasticity and learning in adult mice. Cell Stem Cell. 12:342–353.

Hirase H, Qian L, Bartho P, Buzsaki G. 2004. Calcium dynamics of cortical astrocytic networks in vivo. PLoS Biol. 2:E96.

Iadecola C, Nedergaard M. 2007. Glial regulation of the cerebral microvasculature. Nat Neurosci. 10:1369–1376.

Jabs R, Pivneva T, Huttmann K, Wyczynski A, Nolte C, Kettenmann H, Steinhauser C. 2005. Synaptic transmission onto hippocampal glial cells with hGFAP promoter activity. J Cell Sci. 118:3791–3803.

Jiang P, Chen C, Wang R, Chechneva OV, Chung SH, Rao MS, Pleasure DE, Liu Y, Zhang Q, Deng W. 2013. hESC-derived Olig2+ progenitors generate a subtype of astroglia with protective effects against ischaemic brain injury. Nat Commun. 4:2196.

Krencik R, Weick JP, Liu Y, Zhang ZJ, Zhang SC. 2011. Specification of transplantable astroglial subtypes from human pluripotent stem cells. Nat Biotechnol. 29:528–534.

Kuchibhotla KV, Lattarulo CR, Hyman BT, Bacskai BJ. 2009. Synchronous hyperactivity and intercellular calcium waves in astrocytes in Alzheimer mice. Science. 323:1211–1215.

Kuga N, Sasaki T, Takahara Y, Matsuki N, Ikegaya Y. 2011. Large-scale calcium waves traveling through astrocytic networks in vivo. J Neurosci. 31:2607–2614.

Kunzelmann P, Schroder W, Traub O, Steinhauser C, Dermietzel R, Willecke K. 1999. Late onset and increasing expression of the gap junction protein connexin30 in adult murine brain and long-term cultured astrocytes. Glia. 25:111–119.

Lai CS, Franke TF, Gan WB. 2012. Opposite effects of fear conditioning and extinction on dendritic spine remodelling. Nature. 483:87–91.

Lakoma J, Garcia-Alonso L, Luque JM. 2011. Reelin sets the pace of neocortical neurogenesis. Development. 138:5223–5234.

Lepore AC, Rauck B, Dejea C, Pardo AC, Rao MS, Rothstein JD, Maragakis NJ. 2008. Focal transplantation-based astrocyte replacement is neuroprotective in a model of motor neuron disease. Nat Neurosci. 11:1294–1301.

Letzkus JJ, Wolff SB, Meyer EM, Tovote P, Courtin J, Herry C, Luthi A. 2011. A disinhibitory microcircuit for associative fear learning in the auditory cortex. Nature. 480:331–335.

Li H, Li Y, Lei Z, Wang K, Guo A. 2013. Transformation of odor selectivity from projection neurons to single mushroom body neurons mapped with dual-color calcium imaging. Proc Natl Acad Sci USA. 110:12084–12089.

Lindvall O, Kokaia Z. 2006. Stem cells for the treatment of neurological disorders. Nature. 441:1094–1096.

Lopez-Hidalgo M, Schummers J. 2014. Cortical maps: a role for astrocytes?Curr Opin Neurobiol. 24:176–189.

Lukovic D, Stojkovic M, Moreno-Manzano V, Jendelova P, Sykova E, Bhattacharya SS, Erceg S. 2015. Concise review: reactive astrocytes and stem cells in spinal cord injury: good guys or bad guys?Stem Cells. 33:1036–1041.

Maco B, Cantoni M, Holtmaat A, Kreshuk A, Hamprecht FA, Knott GW. 2014. Semiautomated correlative 3D electron microscopy of in vivo-imaged axons and dendrites. Nat Protoc. 9:1354–1366.

Mi H, Barres BA. 1999. Purification and characterization of astrocyte precursor cells in the developing rat optic nerve. J Neurosci. 19:1049–1061.

Mi R, Luo Y, Cai J, Limke TL, Rao MS, Hoke A. 2005. Immortalized neural stem cells differ from nonimmortalized cortical neurospheres and cerebellar granule cell progenitors. Exp Neurol. 194:301–319.

Muller CM, Best J. 1989. Ocular dominance plasticity in adult cat visual cortex after transplantation of cultured astrocytes. Nature. 342:427–430.

Navarrete M, Perea G, Maglio L, Pastor J, Garcia de Sola R, Araque A. 2013. Astrocyte calcium signal and gliotransmission in human brain tissue. Cereb Cortex. 23:1240–1246.

Nedergaard M, Verkhratsky A. 2012. Artifact versus reality–how astrocytes contribute to synaptic events. Glia. 60:1013–1023.

Nimmerjahn A, Kirchhoff F, Kerr JN, Helmchen F. 2004. Sulforhodamine 101 as a specific marker of astroglia in the neocortex in vivo. Nat Methods. 1:31–37.

Panatier A, Vallee J, Haber M, Murai KK, Lacaille JC, Robitaille R. 2011. Astrocytes are endogenous regulators of basal transmission at central synapses. Cell. 146:785–798.

Parpura V, Basarsky TA, Liu F, Jeftinija K, Jeftinija S, Haydon PG. 1994. Glutamate-mediated astrocyte-neuron signalling. Nature. 369:744–747.

Paukert M, Agarwal A, Cha J, Doze VA, Kang JU, Bergles DE. 2014. Norepinephrine controls astroglial responsiveness to local circuit activity. Neuron. 82:1263–1270.

Rodriguez-Arellano JJ, Parpura V, Zorec R, Verkhratsky A. 2016. Astrocytes in physiological aging and Alzheimer's disease. Neuroscience. 26:170–182.

Salter MW, Hicks JL. 1995. ATP causes release of intracellular Ca^{2+} via the phospholipase C beta/IP3 pathway in astrocytes from the dorsal spinal cord. J Neurosci. 15:2961–2971.

Schell MJ, Molliver ME, Snyder SH. 1995. D-serine, an endogenous synaptic modulator: localization to astrocytes and glutamate-stimulated release. Proc Natl Acad Sci USA. 92:3948–3952.

Schulz K, Sydekum E, Krueppel R, Engelbrecht CJ, Schlegel F, Schroter A, Rudin M, Helmchen F. 2012. Simultaneous BOLD fMRI and fiber-optic calcium recording in rat neocortex. Nat Methods. 9:597–602.

Schummers J, Yu H, Sur M. 2008. Tuned responses of astrocytes and their influence on hemodynamic signals in the visual cortex. Science. 320:1638–1643.

Seifert G, Schilling K, Steinhauser C. 2006. Astrocyte dysfunction in neurological disorders: a molecular perspective. Nat Rev Neurosci. 7:194–206.

Seigneur J, Kroeger D, Nita DA, Amzica F. 2006. Cholinergic action on cortical glial cells in vivo. Cereb Cortex. 16: 655–668.

Sekiya T, Holley MC, Hashido K, Ono K, Shimomura K, Horie RT, Hamaguchi K, Yoshida A, Sakamoto T, Ito J. 2015. Cells transplanted onto the surface of the glial scar reveal hidden potential for functional neural regeneration. Proc Natl Acad Sci USA. 112:E3431–3440.

Sharma G, Vijayaraghavan S. 2001. Nicotinic cholinergic signaling in hippocampal astrocytes involves calcium-induced calcium release from intracellular stores. Proc Natl Acad Sci USA. 98:4148–4153.

Shen JX, Yakel JL. 2012. Functional alpha7 nicotinic ACh receptors on astrocytes in rat hippocampal CA1 slices. J Mol Neurosci. 48:14–21.

Silver J, Miller JH. 2004. Regeneration beyond the glial scar. Nat Rev Neurosci. 5:146–156.

Smith GM, Silver J. 1988. Transplantation of immature and mature astrocytes and their effect on scar formation in the lesioned central nervous system. Prog Brain Res. 78: 353–361.

Sofroniew MV, Vinters HV. 2010. Astrocytes: biology and pathology. Acta Neuropathol. 119:7–35.

Stosiek C, Garaschuk O, Holthoff K, Konnerth A. 2003. In vivo two-photon calcium imaging of neuronal networks. Proc Natl Acad Sci USA. 100:7319–7324.

Sun W, McConnell E, Pare JF, Xu Q, Chen M, Peng W, Lovatt D, Han X, Smith Y, Nedergaard M. 2013. Glutamate-dependent neuroglial calcium signaling differs between young and adult brain. Science. 339:197–200.

Takano T, Tian GF, Peng W, Lou N, Libionka W, Han X, Nedergaard M. 2006. Astrocyte-mediated control of cerebral blood flow. Nat Neurosci. 9:260–267.

Thrane AS, Rangroo Thrane V, Zeppenfeld D, Lou N, Xu Q, Nagelhus EA, Nedergaard M. 2012. General anesthesia selectively disrupts astrocyte calcium signaling in the awake mouse cortex. Proc Natl Acad Sci USA. 109:18974–18979.

Ventura R, Harris KM. 1999. Three-dimensional relationships between hippocampal synapses and astrocytes. J Neurosci. 19:6897–6906.

Volterra A, Liaudet N, Savtchouk I. 2014. Astrocyte Ca(2)(+) signalling: an unexpected complexity. Nat Rev Neurosci. 15:327–335.

Volterra A, Meldolesi J. 2005. Astrocytes, from brain glue to communication elements: the revolution continues. Nat Rev Neurosci. 6:626–640.

Wang X, Lippi G, Carlson DM, Berg DK. 2013. Activation of alpha7-containing nicotinic receptors on astrocytes triggers AMPA receptor recruitment to glutamatergic synapses. J Neurochem. 127:632–643.

Wang X, Lou N, Xu Q, Tian GF, Peng WG, Han X, Kang J, Takano T, Nedergaard M. 2006. Astrocytic Ca2+ signaling evoked by sensory stimulation in vivo. Nat Neurosci. 9:816–823.

Wang X, Takano T, Nedergaard M. 2009. Astrocytic calcium signaling: mechanism and implications for functional brain imaging. Methods Mol Biol. 489:93–109.

Wenk GL. 1997. The nucleus basalis magnocellularis cholinergic system: one hundred years of progress. Neurobiol Learn Mem. 67:85–95.

Wilke SA, Antonios JK, Bushong EA, Badkoobehi A, Malek E, Hwang M, Terada M, Ellisman MH, Ghosh A. 2013. Deconstructing complexity: serial block-face electron microscopic analysis of the hippocampal mossy fiber synapse. J Neurosci. 33:507–522.

Witcher MR, Kirov SA, Harris KM. 2007. Plasticity of perisynaptic astroglia during synaptogenesis in the mature rat hippocampus. Glia. 55:13–23.